

Suzaku Observations of the Supernova Remnant N23 in the Large Magellanic Cloud

Kentaro SOMEYA^{1*}, Aya BAMBA^{2,1}, and Manabu ISHIDA¹

¹*Institute of Space and Astronautical Science/JAXA, 3-1-1 Yoshinodai, Chuo-ku, Sagami-hara, Kanagawa 252-5210, Japan*

²*School of Cosmic Physics, Dublin Institute for Advanced Studies, 31 Fitzwilliam Place, Dublin 2, Ireland*
someya@astro.isas.jaxa.jp

(Received 2000 December 31; accepted 2001 January 1)

Abstract

X-ray emission from the supernova remnant N23 in the Large Magellanic Cloud (LMC) is studied using the X-ray Imaging Spectrometer (XIS) onboard Suzaku. Thanks to superior energy resolution of the XIS in the soft X-ray band, we resolved H-like and He-like Oxygen $K\alpha$ emission lines from N23 with unprecedentedly high quality, and as a result, identified a new optically thin thermal emission component with a temperature ~ 0.2 keV, as well as that with a temperature of ~ 0.5 – 0.7 keV previously known. This alters the estimate of the ionization timescale $n_e t$ from $\sim 10^{10-11}$ cm^{-3} s to $\gtrsim 10^{12}$ cm^{-3} s. Under the assumption that N23 is still in the Sedov phase, its age evaluated from the newly discovered low temperature component is ~ 8000 yr, although it is possible that N23 has already moved into the radiative phase. The abundances of the heavy elements are found to be roughly consistent with those of the LMC average, which indicates that the origin of the X-ray emission of N23 is swept-up ambient material, as expected from its ionization timescale.

Key words: ISM: individual (N23) — shock waves — supernova remnants — X-ray: ISM

1. Introduction

Chemical evolution of the universe has been one of the major issues in the modern astronomy. Heavy elements, or metals, have been generated and accumulated in the universe since its birth mainly through supernovae. An important clue to understand the chemical evolution of the universe will no doubt be brought about by systematic study of a well-defined sample of supernova remnants. In X-ray observations, we are able to extract information of plasma temperature, metal abundance, explosion energy, ionization age, and so on from optically thin thermal plasma emission from supernova remnants (SNRs). These pieces of information will lead to understand galactic chemical evolution and star formation history. A systematic study of SNRs in the Large Magellanic Cloud (LMC) suits well for this purpose, because of its well-known distance (50kpc; Feast 1999) and small interstellar absorption to LMC. The fact that LMC is face-on to us is another advantage. Because of these characteristics, systematic X-ray studies of the thermal SNRs in LMC have been carried out with some major X-ray observatories (e.g. Hughes et al. 1998). These observations are, however, limited in terms of energy resolution in the low energy band below ~ 1 keV, which is important to study the nature of the SNR plasma in detail, because the temperature of the plasma in most SNRs is less than ~ 2 keV. In particular, hydrogenic and He-like Oxygen $K\alpha$ lines that appear in 0.5–0.7 keV dominate a spectrum of the

plasma with a temperature of $\lesssim 1$ keV, and hence, high resolution spectroscopy in this energy band is of great importance in evaluating the parameters of the low temperature plasma, such as the temperature, the density, the ionization parameter and the abundances of the metal. We therefore have decided to perform a systematic study of the SNRs in LMC with the Suzaku XIS (Mitsuda et al. 2007, Koyama et al. 2007), which has the best energy resolution in the Oxygen 0.5–0.7 keV energy band among the CCDs currently in orbit. In this paper, we study the SNR N23, as a beginning of our systematic study project.

N23 is identified as a SNR with radio observations at 5 and 14.7 GHz for the first time (Milne et al. 1980). Its X-ray emission extends $100'' \times 120''$ in the sky (24×29 pc at a distance of 50 kpc), showing a semi-circular morphology with only the south-eastern hemisphere being bright (Hughes et al. 2006). Based on the ASCA observation, Hughes et al. (1998) classified N23 as a young SNR with an age of ~ 3800 from the spectrum of the entire remnant. Hughes et al. (2006) carried out spatially resolved spectroscopy of N23 with Chandra, and estimated the age of north-western rim to be ~ 4600 yr. These observations result in consistent estimation of the temperature and the ionization parameter ($n_e t$) in the bright south-eastern shell, which is ~ 0.5 – 0.7 keV and $\sim 10^{10}$ – 10^{11} cm^{-3} s, respectively. They are, however, not be able to resolve hydrogenic and He-like $K\alpha$ lines from Oxygen clearly because of limited energy resolution below ~ 1 keV. In addition, Hughes et al. (2006) have revealed that there is a point source around the center of N23. From its 0.5–10 keV flux ($\sim 10^{-14}$ $\text{erg cm}^{-2} \text{s}^{-1}$) and power-law spectrum with a photon index of 2.2, the source is probably a

* Department of Physics, Tokyo Institute of Technology, 2-12-1 Ookayama, Meguro-ku, Tokyo 152-8551, Japan

rotation-powered pulsar and/or a pulsar wind nebula. If so, the progenitor of N23 is a core-collapsed massive star (Hayato et al. 2006).

This paper is organized as follows. After describing how the observation and data reduction are carried out in § 2, we report the results of spectral analysis of N23 in § 3. Owing to high spectral resolution of the XIS in the Oxygen $K\alpha$ band, we have clearly resolved hydrogenic and He-like $K\alpha$ emission lines from Oxygen for the first time, which leads to identification of a new low temperature component. Based on these results, we discuss the plasma parameters and evolutionary phase of N23 in § 4. Finally, the summary is given in § 5.

2. Observation and Data Reduction

N23 was observed with Suzaku (Mitsuda et al. 2007) on 2005 August 16–17. The observation log is summarized in table 1. Suzaku is equipped with four modules

Table 1. observation log.

Observation ID	100003010
Observation mode	Full window, no burst, no SCI
Start Date (UT)	2005/08/16–17
Exposure (ksec)	7.1
Count rate* (cts s ⁻¹)	FI: 0.6 BI: 1.2

* Count rate of FI and BI-CCD. Count rate of N23 in the 0.5–2.0 band within a 3'.3 radius circle after the background subtraction.

of the XIS (Koyama et al. 2007). One of them adopts a back-illuminated CCD (BI-CCD), which is referred to as XIS1 having superior quantum efficiency especially in a low energy band, whilst the other three modules (XIS0, XIS2 and XIS3) utilize front-illuminated (FI) CCDs which have high sensitivity in a high energy band and better energy resolution than the BI-CCD. They are adapted at the focal plane of the X-Ray Telescopes (XRT; Serlemitsos et al. 2007). They are thin-foil-nested X-ray mirrors realizing a high throughput in 0.2–12 keV with a moderate imaging capability (1'.8–2'.3 in half-power diameter). The Suzaku XIS image of N23 below 2 keV is shown in Fig. 1.

Data reduction and analysis of the present data were carried out using the HEADAS software package version 6.5.1. The data processed by Suzaku pipeline processing software (ver 2.0) were analyzed. We only used the data taken with the 5 × 5 editing mode in the high and super-high data rates because of the editing mode of 2 × 2 has uncertainty in the response matrices of the XIS. In screening the data, we removed time intervals while the elevation angle from the night earth is less than 5°. In the standard data screening procedure, the time interval during which the elevation angle from the day earth is less than 20°. This results in, however, only 5.6 ksec data available. We thus reduce the day-earth elevation angle by degrees by closely comparing resulting spectra and have finally found that the solar X-ray contamination does not raise any spectral modification even if we reduce the day

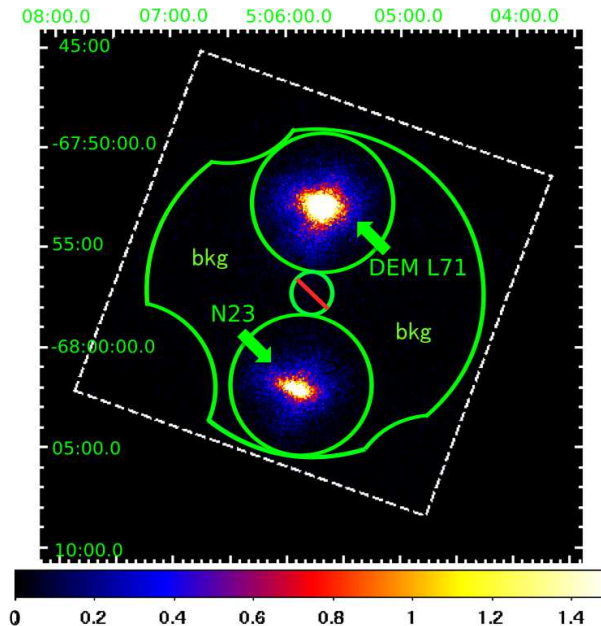


Fig. 1. Suzaku XIS X-ray image of the N23 in the bands 0.2–2 keV. Another nearby SNR, DEM L71, is also shown. The images from all the four XIS modules are combined. The green circles with a radius of 3'.3 are integration regions of the source photons from N23. The background photons were extracted from annular region which was removed the source and a center regions. The calibration sources at the corners are masked.

earth elevation down to 5° (DYE_ELV > 5°) for the XIS data. Owing to this study, the total exposure time has increased to 7.1 ksec.

3. Spectral Analysis

3.1. Extraction of Source and Background Photons

In extracting source photons, we adopt a circular aperture with a radius of 3'.3 centered on N23 (the green circle centered on N23 in Fig. 1). For the background, we have collected photons from the entire CCD area out of the source extraction region, except for outer edge regions illuminated by ⁵⁵Mn isotopes adapted in the camera bodies of all the XIS modules, the central circular region with a radius of ~1'.5, and the 3'.3 circular region centered on the other SNR DEM L71. We combined the spectra from the XIS adopting the FI-CCDs (XIS0, XIS2, and XIS3) into a single spectrum, and refer to it as the FI spectrum hereafter. The BI spectrum is the same as that solely from the XIS1 data.

In the spectral analysis, we use XSPEC version 11.3.2aj. The XIS response matrix (RMF) and auxiliary response file (ARF) are calculated using XISRMFGEN (version 2007-05-14) and XISARFGEN (version 2008-04-05), respectively (Ishisaki et al. 2007). The RMFs and ARFs from the FI-CCDs are combined with the ftools ADDRMF and MARFRMF.

3.2. Spectral Models

From the ASCA observations of LMC SNRs, it is found that the spectra of N23 is well represented by an optically thin thermal emission model in ionization non-equilibrium (Hughes et al. 1998). In characterizing the spectra of SNR, we thus adopt the non-equilibrium ionization model, or VNEI model in the XSPEC model library. The VNEI model provides the plasma temperature kT_e , the ionization timescale $n_e t$ where t is the elapsed time since the shock occurs, the metal abundances, and the normalization parameter $\frac{10^{-14}}{4\pi D^2} \int n_e n_H dV$ where D is the distance to the source, n_e and n_H are the electron and hydrogen density respectively, and dV is the volume element of the SNR.

The emission spectra are attenuated by photoelectric absorption due to metals contained in the interstellar matter within our galaxy and LMC. Since the metal abundances of these two absorption components are significantly different, we consider them separately in the spectral evaluation as follows. We assume solar composition (Anders & Grevesse 1989) for the absorbing matter in the Galaxy, and denote its hydrogen column density as N_H^G . The value of N_H^G toward N23 is obtained by the Galactic HI survey, which is $5.8 \times 10^{20} \text{cm}^{-2}$ (Dickey & Lockman 1990). We utilize the PHABS model in XSPEC to represent the galactic absorption, and freeze N_H^G at these values in the spectral fitting described below. The average metal abundances of LMC, on the other hand, are measured by Russell & Dopita (1992), which is ~ 0.3 solar on average over major metals. We reflect these abundances on the VPHABS model, and set the column density associated with LMC N_H^L free to vary in the following spectral fit process.

In evaluating the spectrum of N23 through spectral fitting, we begin with a single component VNEI model attenuated by photoelectric absorption. Since the carbon abundance cannot be constrained because of the large interstellar absorption at carbon $K\alpha$ line energies, we fixed it to the LMC value (Russell & Dopita 1992). In the early phase of the Suzaku mission, the energy gain has a large uncertainty (Koyama et al. 2007). The gain uncertainty is $\sim \pm 10$ eV, according to the previous studies on SNRs (Bamba et al. 2008; Yamaguchi et al. 2008). We therefore have allowed the energy offset to be floated. As a result, the energy offset is converged to ~ -8 eV and ~ -1 eV, for the FI and BI spectra, respectively. These gain offset values are within the gain uncertainty. The result is summarized in the second column of table 2 labelled ‘ $1kT1nt$ ’. The best fit results in $kT_e \simeq 0.548$ keV and $\log(n_e t [\text{cm}^{-3} \text{s}]) \simeq 10.51$ with a χ^2 (d.o.f.) of 144 (99). These parameters are roughly consistent with those from the Chandra observation. Note that, if we do not float the energy gain, the best-fit parameters are $kT_e \simeq 0.552$ keV and $\log(n_e t [\text{cm}^{-3} \text{s}]) \simeq 10.54$ with a χ^2 (d.o.f.) of 219 (101). Hence, the energy offset adjustment significantly improves the fit, while the differences in the temperature and the ionization timescale (in logarithm) are within ~ 1 %.

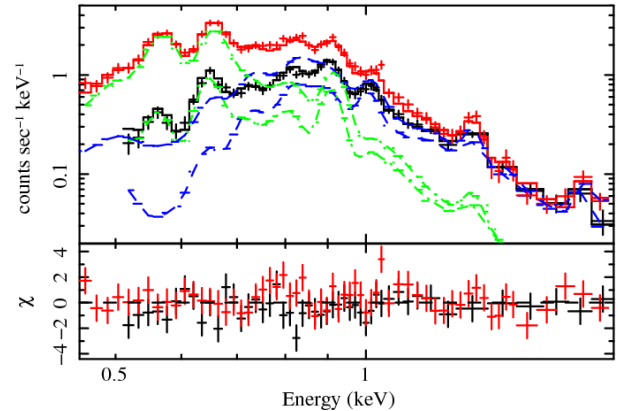


Fig. 2. The data and the best-fit ‘ $2kT1nt$ ’ model of N23. in the 0.45–2.0 keV band. The black and red crosses show the data point from the FI and BI CCDs, respectively. The solid histograms with the same color are the best-fit model. The blue and green broken histograms show the components with $kT_e=0.57$ and 0.22 keV, respectively. The lower panel shows the residuals from the best-fit model.

As noticed from this table, however, the single component VNEI model no longer provides an acceptable fit ($\chi^2_\nu \simeq 1.5$). We thus have appended another VNEI model. To reduce the number of model parameters as much as possible, we constrained either kT_e or $n_e t$ common between the two VNEI components, and fit them to the data separately. The resultant best-fit parameters are also listed in table 2, labelled ‘ $1kT2nt$ ’ and ‘ $2kT1nt$ ’, respectively. Although the $1kT2nt$ model improves the fit significantly, the reduced χ^2 value indicates that it is still not acceptable. The improvement of the $2kT1nt$ model, on the other hand, is more remarkable, and it provides an acceptable fit at the 90% confidence level. The best-fit model is shown in Fig. 2. This result indicates that there exists another optically thin thermal plasma component with a temperature of ~ 0.2 keV, in addition to the 0.5–0.6 keV component so far known. The discovery of the new low temperature component is brought about by the clear resolution of the Oxygen $K\alpha$ lines by the Suzaku XIS. Consequently, the best-fit value of the ionization timescale now becomes $\log(n_e t [\text{cm}^{-3} \text{s}]) \gtrsim 12$. This is significantly larger than that from the ASCA and Chandra observations ($10^{10} - 10^{11} \text{cm}^{-3} \text{s}$).

In the Chandra observation, more than ~ 30 % of the total emission comes from the eastern rim (Hughes et al. 2006). Since our Suzaku observation covers the remnant entirely, the best-fit parameters we have obtained are a kind of mean weighted mainly on this extended bright rim region (see Fig. 3).

We finally remove the constraint of the ionization timescale between the two VNEI components and set them free to vary independently. The results are summarized in the ‘ $2kT2nt$ ’ column of table 2. This change, however, is not effective in improving the fit. We therefore adopt the $2kT1nt$ model for N23 for discussion in later sections.

Table 2. Best-fit parameters for N23*.

Parameters	1kT1nt	1kT2nt	2kT1nt	2kT2nt
$N_{\text{H}}^G (\times 10^{20} \text{ cm}^{-2})$	5.8(fix)	5.8 (fix)	5.8(fix)	5.8(fix)
$N_{\text{H}}^I (\times 10^{21} \text{ cm}^{-2})$	1.6(1.3–1.9)	< 0.16	1.5(0.6–1.9)	0.9(0.6–1.9)
kT_{e1} (keV)	0.548(0.544–0.567)	0.572(0.557–0.580)	0.569(0.556–0.593)	0.581(0.551–0.597)
kT_{e2} (keV)	–	–	0.218(0.214–0.230)	0.225(0.214–0.230)
$\log(n_e t)_1 (\text{cm}^{-3} \text{ s})$	10.51(10.48–10.55)	10.50(10.45–10.52)	13.68(11.92–13.70)	12.04(11.87–13.70)
$\log(n_e t)_2 (\text{cm}^{-3} \text{ s})$	–	13.18(12.77–13.70)	–	13.63(13.27–13.70)
$Norm_1^\dagger (\times 10^{-2})$	1.87(1.74–1.90)	0.34(0.31–0.68)	0.83(0.64–1.00)	0.78(0.66–0.98)
$Norm_2^\dagger (\times 10^{-2})$	–	0.73(0.67–0.81)	2.54(1.93–2.96)	1.93(1.47–3.51)
C	0.30(fix)	0.30(fix)	0.30(fix)	0.30(fix)
N	< 0.02	0.09(0.04–0.25)	0.54(0.12–1.05)	0.37(0.23–0.94)
O	0.093(0.089–0.098)	0.27(0.26–0.28)	0.33(0.25–0.50)	0.34(0.28–0.49)
Ne	0.15(0.14–0.16)	0.43(0.39–0.46)	0.49(0.35–0.70)	0.49(0.40–0.66)
Mg	0.14(0.12–0.17)	0.31(0.27–0.35)	0.39(0.33–0.60)	0.39(0.32–0.47)
Si	0.28(0.19–0.36)	0.34(0.24–0.43)	0.41(0.30–0.52)	0.42(0.32–0.55)
Fe	0.111(0.105–0.117)	0.18(0.17–0.22)	0.24(0.19–0.33)	0.24(0.19–0.33)
$\chi_\nu^2(\text{d.o.f.})$	1.45(99)	1.11(97)	1.00(97)	1.00(96)
offset FI (eV)	–8.7(–11.0––7.8)	–8.1(–9.1––5.9)	–8.1(–9.0––7.1)	–8.0(–9.0––7.1)
offset BI (eV)	–1.0(–1.6– 0.0)	–1.0(–2.1– 0.0)	–1.0(–2.8– 0.0)	–0.3(–1.3– 0.0)

* The errors in the parentheses represent the 90% confidence intervals.

† In units of $10^{-14}/4\pi D^2 \int n_e n_H dV \text{ cm}^{-5}$, where V and D are the Volume and distance to the plasma, respectively.

4. Discussion

4.1. Densities, total energy, and swept up mass

In this section, we aim to derive electron number densities of the SNR plasma (n_e) and ambient ISM (n_0), total thermal energy of the plasma (E_t), swept up mass (M_{swept}). With the aid of the normalization obtained from the spectral fitting, the volume of the plasma (V) and the volume filling factor (f), we calculated n_e , taking into account $n_e = 1.2n_H$ for fully ionized solar abundance plasma. Assuming the strong shock, pre-shock density (e.g. ISM density; n_0) is obtained to be $n_0 = (n_H/4)$. The swept-up mass is given by $M_{\text{swept}} = n_H m_p f V$, where m_p is the proton mass. The total energy is given by $E_t = 3n_e k T f V$, where k and T is the Boltzmann constant and the temperature of the plasma, respectively. Note that we assume that electrons and ions temperature are in thermal equilibrium. The age of the plasma t_{ion} is obtained from the ionization parameter ($n_e t$) which is evaluated from the spectral fitting.

In order to estimate the densities, we need to know the volume of the plasma from an X-ray image. Since the Suzaku XIS has only moderate imaging capability, we carried out Chandra imaging analysis first. We analyzed the Chandra ACIS data of N23 (seq# 500212) observed on 2002 December 29–30. Images are extracted from a standard cleaned event file using the DMCOPY command. Fig. 3 shows the X-ray images in the (a) 0.2–0.8 keV and (b) 1.5–2.0 keV energy bands. The low and high energy bands were chosen to show the contribution from the ~ 0.2 keV and the ~ 0.6 keV components, respectively. In both images, the structure of N23 shows a bright hemisphere with $\sim 35''$ (8.5 pc) radius. We therefore assumed that the N23 plasma distributes in the shell of the hemisphere with a radius and a thickness of $35''$ and $2.7''$

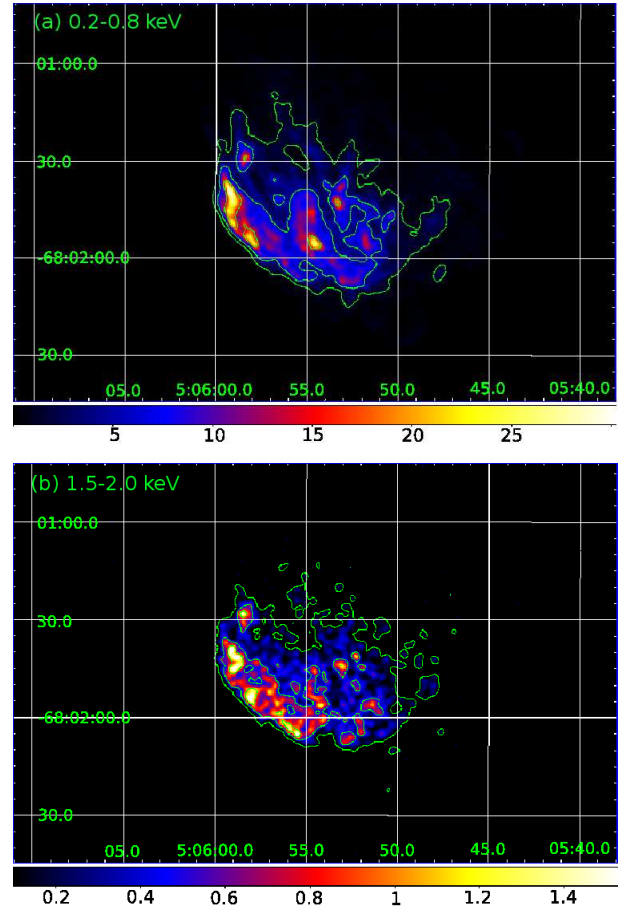


Fig. 3. Smoothed Chandra image of N23 (a) in the 0.2–0.8 keV and (b) in the 1.5–2.0 keV band. The contours overlaid with labels of 1.0, 5.0, 15.0 (left) and 0.1, 0.5, 1.0 counts pixel^{-1}

Table 3. Input and derived properties for N23.

Property	Value	
	low- T component	high- T component
kT_e (keV)	0.22	0.57
R (pc)	8.5	8.5
V (10^{57} cm 3)	9.3	9.3
n_e (cm $^{-3}$)	$31.3^{+2.5}_{-4.1} f_{0.1}^{-1/2}$	$18.0^{+1.6}_{-2.2} f_{0.1}^{-1/2}$
n_0 (cm $^{-3}$)	$7.9^{+0.6}_{-1.0} f_{0.1}^{-1/2}$	$4.4^{+0.3}_{-0.6} f_{0.1}^{-1/2}$
E_t (10^{50} erg)	$0.3 \pm 0.1 f_{0.1}^{1/2}$	$0.4 \pm 0.1 f_{0.1}^{1/2}$
M_{swept} (M_\odot)	$21^{+2}_{-3} f_{0.1}^{1/2}$	$12^{+1}_{-2} f_{0.1}^{1/2}$
t_{ion} (yr)	$> 1000 f_{0.1}^{1/2}$	$> 1500 f_{0.1}^{1/2}$

(0.7 pc), the latter of which is 1/12 of the shell radius expected for the ISM compressed in the case of the strong and adiabatic shock, which assumption is to be considered later in § 4.2. As a result, the volume of the plasma becomes $V = 9.3 \times 10^{57}$ cm 3 .

The other parameters are summarized in table 3. As shown in Fig. 3, the emission from N23 is highly anisotropic. We therefore normalized the volume filling factor f by 0.1 ($\equiv f_{0.1}$). The plasma density estimated from the low and high temperature components are ~ 31 cm $^{-3}$ and ~ 18 cm $^{-3}$, respectively, as shown in table 3. This density estimation is roughly consistent with that of the southeastern rim region with the Chandra observation (~ 10 – 23 cm $^{-3}$; Hughes et al. 2006). With this normalization, the ISM density estimated from the low and high temperature components are ~ 8 cm $^{-3}$ and ~ 4 cm $^{-3}$, respectively. One may imagine that this high density is realized through collision of the ejecta with molecular clouds. According to a radio observation (Banas et al. 1997), however, no CO emission was discovered from a region including N23. We thus consider that N23 explodes into a relatively dense part of the ISM (~ 10 cm $^{-3}$). It is suggested this high density is related geometrically with the open cluster HS 114 (Hodge & Sexton 1966) near the remnant (Hughes et al. 2006). Finally, total ejecta mass is given by $M_{\text{low}} + M_{\text{high}}$, where M_{low} and M_{high} are the mass of low and high temperature components, respectively. Total ejecta mass therefore is calculated to be $\sim 30 M_\odot$. Hence the plasma chiefly comprises of the swept-up ISM.

4.2. SNR phase

In this section, we consider evolutionary phase of N23 by comparing various timescales evaluated from observed parameters. We compare the Sedov time scale (t_{Sedov}), the plasma age (t_{ion}) estimated from the ionization parameter, and the cooling time scale (t_{cool}) of N23. t_{Sedov} is based on the concept of Sedov simple blast wave model (Sedov 1959), in which a supernova with explosion energy (E_0) expands into homogeneous ISM, which is given by

$$t_{\text{Sedov}} = 4.3 \times 10^2 \left(\frac{R}{1 \text{ pc}} \right) \left(\frac{kT_e}{1 \text{ keV}} \right)^{-0.5} \text{ yr}, \quad (1)$$

Table 4. The characteristic ages for N23.

	low- T component	high- T component
t_{Sedov} (10^4 yr)	0.8	0.5
t_{cool} (10^4 yr)	$0.9 f_{0.1}^{0.26}$	$1.2 f_{0.1}^{0.26}$
t_{ion} (10^4 yr)	$> 0.1 f_{0.1}^{1/2}$	$> 0.2 f_{0.1}^{1/2}$

where R is the blast wave shock radius and T_e is the shock temperature. t_{cool} is defined as the time scale of the temperature distribution having started to deviate from that of the Sedov model, which is written as

$$t_{\text{cool}} = 2.7 \times 10^4 \left(\frac{E_0}{10^{51} \text{ erg}} \right)^{0.24} \left(\frac{n_0}{1 \text{ cm}^{-3}} \right)^{-0.52} \text{ yr} \quad (2)$$

(Falle 1981). If $t_{\text{cool}} \simeq t_{\text{Sedov}}$ holds, the SNR is considered to locate at a late stage of the Sedov phase or at an initial radiative phase. If, on the other hand, $t_{\text{Sedov}} < t_{\text{cool}}$ holds, the SNR is regarded as being still in the Sedov phase. We assume that the explosion energy is 10^{51} erg in eq. (2).

We discovered the new soft emission component with a temperature of ~ 0.22 keV, in addition to the 0.5–0.7 keV component so far known. Accordingly, we need to update the remnant age estimation. The Sedov time scale and the cooling time scale calculated with eq. (1) and (2) are summarized in table 4, together with the ionization age t_{ion} obtained based on the spectral fit. Since the spectral fit with the ‘ $2kT1nt$ ’ model provides only the lower limit for the ionization timescale $n_e t$, we only have a lower limit for t_{ion} . We thus have decided to estimate the remnant age with eq. (1) and (2). Using eq. (1) with $R = 8.5$ pc, t_{Sedov} estimated from the low and high temperature components becomes ~ 8000 and ~ 5000 yr, respectively, which are consistent with the lower limit of t_{ion} . This is a direct consequence of eq. (1), implying t_{Sedov} being proportional to $T_e^{-1/2}$. The high temperature component is younger than the low temperature component. In the Sedov scheme, this can be interpreted as the high temperature component being heated recently. On the other hands, t_{cool} of the low and high temperature components are $9300 f_{0.1}^{0.26}$ and $12000 f_{0.1}^{0.26}$, respectively, using eq. (2) with n_0 given in table 3 (§4.1). Since $t_{\text{Sedov}} \lesssim t_{\text{cool}}$ for both components, N23 is likely to be at a late stage of the Sedov phase, and if so, its age is ~ 8000 yrs old from the newly discovered low temperature component.

Note, however, that this discussion depends on the estimation of the volume filling factor f . Accounting for the highly anisotropic image (Fig. 3), we have normalized f by 0.1. However, if the shock wave of N23 propagates in a higher density ISM, like the edge of the open cluster HS 114 (Hodge & Sexton 1966), the total volume should be smaller for the given emission measure, resulting in a smaller f . If, for instance, $f = 0.01$, t_{cool} of the low and high temperature components are ~ 5000 and ~ 7000 yr, respectively. Since $t_{\text{cool}} \lesssim t_{\text{Sedov}}$, the low temperature component should be regarded as in the radiative phase. In addition, we would also like to remark that, in § 4.1,

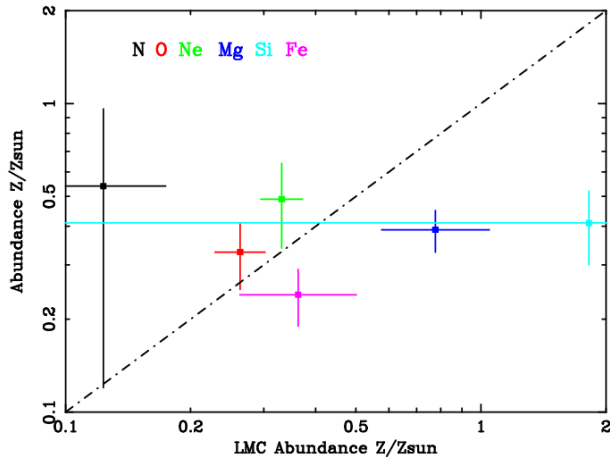


Fig. 4. Elemental abundance as derived from fits to the XIS data. The derived N23 abundance value is the square. The ratios are all relative to solar (Andres & Grevesse 1989). The silicon abundance in Russell & Dopita’s work is highly uncertain as indicated by our use of a large error bar for this species. Dashed line represents the abundance in these SNRs are same to the LMC average.

we have calculated the plasma volume, assuming that the shell thickness is 1/12 of the shell radius, which is expected for a spherical strong shock. This holds only if N23 is still in the Sedov (adiabatic) phase. If N23 has been in the radiative phase, then the shell thickness should be smaller due to radiative cooling, and hence, the plasma density would be larger than the current estimation. As a result, the cooling time scale estimated from eq. (2) should be smaller, and $t_{\text{cool}} \lesssim t_{\text{Sedov}}$. Consequently, we cannot deny possibility that N23 has been in the radiative phase.

In summary, the age of N23 is estimated to be ~ 8000 yr from the newly discovered low temperature component as long as it still stays in Sedov phase. This condition is, however, uncertain, because the discussion depends on the volume filling factor of the plasma. If, for instance, the shock propagate in the higher density ISM, N23 may have already entered into the radiative cooling phase. In this case, the remnant age estimated from the cooling timescale is smaller.

Finally, we can make an independent age estimation from the central source detected by Chandra (Hayato et al. 2006). Its luminosity is 1×10^{34} erg in the 0.5–10.0 keV (Hayato et al. 2006). If the central source is a pulsar (although the pulsation has not been detected), the characteristic age is $\sim 10^3$ – $10^{4.5}$ years (Possenti et al. 2002), which is consistent with our age estimation update.

4.3. Abundance

The main component of X-ray emission originates from the swept-up ISM in N23. Hence the elemental abundances of N23 reflect those of its environment. Figure 4 shows the abundances obtained from the spectral analysis (table 2). The abundances of N, O, Ne and Fe agree roughly with the LMC average (Russell & Dopita 1992). The Si and Mg abundances are smaller than those ob-

tained (Russell & Dopita 1992), although their errors are relatively large. The Mg and Si abundances obtained by Suzaku are consistent with those from ASCA (Hughes et al. 1998), respectively, which seem slightly less than the LMC average.

5. SUMMARY

We observed N23 in the Large Magellanic Cloud with Suzaku, and discovered the new soft emission component with a temperature of ~ 0.22 keV, in addition to the ~ 0.5 – 0.7 keV component so far known. This alters the estimate of the ionization parameter ($n_e t$) significantly from $\sim 10^{10}$ – 10^{11} cm^{-3} s to $\gtrsim 10^{12}$ cm^{-3} s. With the aid of Chandra imaging capability, we are able to calculate the density of the plasma, and have confirmed that the supernova explosion of N23 occurred in a high density region with an ISM density of ~ 4 – 8 cm^{-3} . The relatively high ambient density may be related to the open cluster HS 114 (Hodge & Sexton 1966) near the remnant (Hughes et al. 2006). The parameters of the plasma from our analysis indicate that N23 is either at a late stage of the Sedov phase or in the radiative cooling phase. Assuming it is still in the Sedov phase, we have estimated the age of the remnant to be ~ 8000 yr from the newly discovered soft component, which is twice as old as the estimation by Hughes et al. (1998). Given the uncertainty of the volume filling factor, however, we cannot deny the possibility that N23 has already entered into the radiative phase.

The abundances of N23 is roughly consistent with the LMC average (Russell & Dopita 1992). The Si and Mg abundances obtained by spectral fitting are smaller than those obtained by Russell & Dopita (1992), although their errors on Si and Mg abundances are relatively large. The Mg and Si abundances obtained by Suzaku are consistent with those from ASCA (Hughes et al. 1998).

We thank Dr. Y. Maeda for his useful discussion and comments. We would like to express our gratitude to all members of the Suzaku team for their contributions to the instrument preparation, spacecraft operation, software development, and in-orbit instrumental calibration. We also thank an anonymous referee for useful comments.

References

- Anders, E., & Grevesse, N. 1989, *Geochim. Cosmochim. Acta*, 53, 197
- Bamba, A., et al. 2008, *PASJ*, 60, 153
- Banas, K. R., Hughes, J. P., Bronfman, L., & Nyman, L.-A. 1997, *ApJ*, 480, 607
- Dickey, J. M., & Lockman, F. J. 1990, *ARA&A*, 28, 215
- Falle, S. A. E. G. 1981, *MNRAS*, 195, 1011
- Feast, M. 1999, *PASP*, 111, 775
- Hayato, A., Bamba, A., Tamagawa, T., & Kawabata, K. 2006, *ApJ*, 653, 280
- Hodge, P. W., & Sexton, J. A. 1966, *AJ*, 71, 363
- Hughes, J. P., Hayashi, I., & Koyama, K. 1998, *ApJ*, 505, 732
- Hughes, J. P., Rafelski, M., Warren, J. S., Rakowski, C., Slane, P., Burrows, D., & Nousek, J. 2006, *ApJL*, 645, L117

- Ishisaki, Y., et al. 2007, PASJ, 59, 113
Koyama, K., et al. 2007, PASJ, 59, 23
Milne, D. K., Caswell, J. L., & Haynes, R. F. 1980, MNRAS,
191, 469
Mitsuda, K., et al. 2007, PASJ, 59, 1
Possenti, A., Cerutti, R., Colpi, M., & Mereghetti, S. 2002,
A&A, 387, 993
Russell, S. C., & Dopita, M. A. 1992, ApJ, 384, 508
Sedov, L. I. 1959, Similarity and Dimensional Methods in
Mechanics, New York: Academic Press, 1959,
Serlemitsos, P. J., et al. 2007, PASJ, 59, 9
Yamaguchi, H., et al. 2008, PASJ, 60, 141